Radiative divertor behavior and physics in Ar seeded plasma on EAST*

Jingbo Chen(陈竞博)[1,2], Yanmin Duan(段艳敏)[1], Zhongshi Yang(杨钟时)[1,2,†], Liang Wang(王亮)[1], Kai Wu(吴凯)[1,2], Kedong Li(李克栋)[1,2], Fang Ding(丁芳)[1], Hongmin Mao(毛红敏)[1], Jichan Xu(许吉禅)[1,2], Wei Gao(高伟)[1], Ling Zhang(张凌)[1], Jinhua Wu(吴金华)[1], Guang-Nan Luo(罗广南)[1,2], and EAST Team[1]

[1] *Institute of Plasma Physics, Chinese Academy of Sciences, Hefei* 230031, *China*
[2] *Science Island Branch of Graduate School, University of Science & Technology of China, Hefei* 230031, *China*

(Received 11 April 2017; revised manuscript received 26 May 2017; published online 31 July 2017)

To investigate the radiative divertor behavior and physics for the scenario of impurity seeded plasma in ITER, the radiative divertor experiments with argon (Ar) seeding under ITER-like tungsten divertor condition were carried out during recent EAST campaigns. The experimental results reveal the high efficiency of reducing heat load and particle flux onto the divertor targets owing to increased radiation by Ar seeding. We achieve detached plasmas in these experiments. The inner–outer divertor asymmetry reduces after Ar seeding. Impurities, such as Ar, C, Li, and W, exist in the entire space of the vacuum chamber during EAST operations, and play important roles in power exhausting and accelerating the plasma detachment process. It is remarkable that the contamination of the core plasma is observed using Ar seeding owing to the sputtering of plasma facing components (PFCs), particularly when Ar impurity is injected from the upper tungsten divertor.

Keywords: argon seeding, power exhaust, ITER-like tungsten divertor, EAST

PACS: 52.55.Rk, 52.25.Vf, 52.40.Hf, 52.55.Fa **DOI:** 10.1088/1674-1056/26/9/095205

1. Introduction

Increasing divertor radiation by injecting impurity is a general and effective method for reducing the heat flux from the scrape-off layer and for cooling the divertor plasma to detachment. Impurities, such as nitrogen (N_2), neon (Ne) and argon (Ar), are widely used in radiative divertor experiments on several tokamaks. In ASDEX Upgrade with full tungsten divertor wall conditions, complete and partial detached plasmas were achieved by feedback controlled N_2 seeding. In addition, Ar or Ne impurities were also used to control the heat flux onto the divertor successfully.[1,2] In JET, N_2 seeding was used for comparing the effect of reducing the heat load on the ITER-like wall (ILW) to that on all-carbon wall conditions. The experiment results, such as increasing the plasma density and reducing the ELM frequency and pedestal pressure with N_2 seeding between two divertors, were clearly different.[3] In JT-60U, with Ne, Ar, and a mixture of Ne and Ar injection in H-mode plasmas, the fractions of divertor radiation power by these impurities besides an intrinsic impurity, C, were investigated. It was found that Ne is the dominant radiator when plasma detached by Ne seeding, but carbon acts as the biggest radiator with other impurities seeding in carbon wall conditions.[4]

The EAST has previously achieved a minute-scale non-inductive H-mode in the 2016 campaign. It aims at obtaining a long pulse discharge over 1000 s with high-performance plasma in the future. In this situation, the EAST divertor faces a severe challenge owing to high heat flux; therefore, the radiative divertor experiments were conducted and investigated. Furthermore, EAST upgraded its upper divertor into actively cooled W/Cu plasma-facing components (PFCs) in 2014.[5,6] Some divertor behavior as demonstrated in the carbon divertor before is necessary to be validated in the ITER-like tungsten divertor. Owing to the routine lithium wall coating conditioning before EAST discharges, Ar, instead of N_2 which easily reacts with hydrogen and lithium, was used as the seeded impurity for achieving long-pulse high-performance operations in EAST.[7–9] In this study, we introduce the radiative divertor experiments conducted during EAST 2014 and 2015 campaigns by using the mixture of Ar/D_2 (1:4) as the seeded impurity. These experiments are primarily focused on investigating the divertor heat load reduction, radiation distribution, asymmetry evolution, and impurities behavior under tungsten wall conditions. From the results of the experiment, Ar proved to have high efficiency in reducing heat and particle fluxes onto the divertor targets. However, excessive Ar seeding that easily caused contamination in the core plasma region is discussed in Section 3. The asymmetry between the inner and outer divertor is described in Section 3.2. Impurities, such as Ar, C, Li, and W, induced by impurity injection, play important roles in power exhausting and accelerating the plasma detachment process as described in Section 3.3. A summary is provided in the final section.

*Project supported by the National Natural Science Foundation of China (Grant Nos. 11575242, 11575243, 11505233, 11575247, and 11605238) and the National Magnetic Confinement Fusion Science Program (Grant Nos. 2013GB105002 and 2013GB105001).

†Corresponding author. E-mail: zsyang@ipp.ac.cn

© 2017 Chinese Physical Society and IOP Publishing Ltd

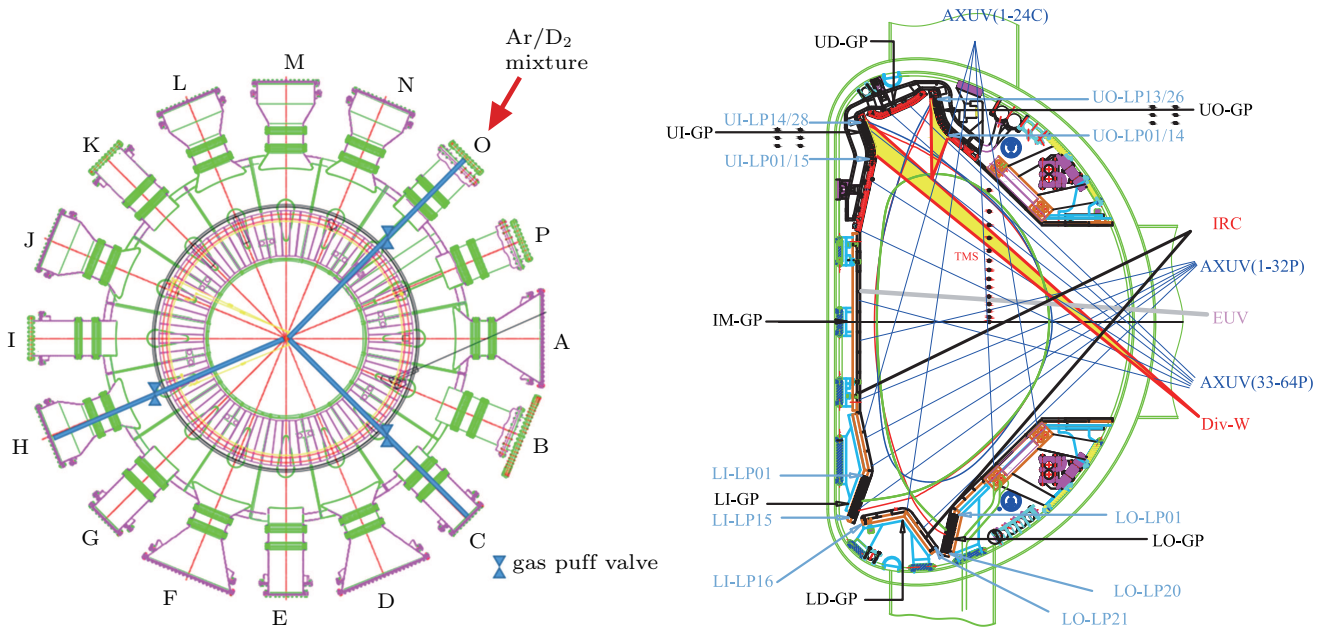


Fig. 1. (color online) Toroidal and poloidal cross section of EAST showing relevant diagnostics of experiments and divertor gas puff locations. AXUV: absolute extreme ultraviolet bolometer arrays; U(L)I: upper (lower) inboard divertor; U(L)O: upper (lower) outboard divertor; U(L)D: upper (lower) divertor dome; GP: gas puff inlet; IM: inner midplane; TMS: Thomson scattering; IRC: infrared camera; EUV: extreme ultraviolet spectrometer; Div-W: divertor tungsten spectroscopy.

2. Experimental setup and relevant diagnostics

During 2014 and 2015 EAST campaigns, radiative divertor experiments were conducted in both L-mode and H-mode discharges in order to compare the differences between these two confinement modes, particularly for heat load reduction, radiation, inboard–outboard asymmetry, and impurities transport behaviors in the divertor region. As shown in Fig. 1, the controlled pulsed mixture of Ar/D_2 (1:4) was injected through a pipe located inside the divertor target near the strike point. The delay time of Ar affecting the divertor plasma was approximately 75–140 ms limited by the length of pipes after the upgrade of the divertor gas puff system in 2014.[10] The width of puffing pulse was controlled using the plasma control system (PCS) program setting. According to different divertor configurations (lower single null (LSN) and upper single null (USN) configuration), the mixture was injected from different regions, that is, lower carbon divertor and upper ITER-like tungsten divertor, in several discharges. The results are discussed in Section 3.

Table 1. Coordinates of gas puff inlet.

Location		R/m	Z/m
Upper divertor	Outer	1.725	1.083
	Inner	1.407	0.974
	Dome	1.558	1.061
Lower divertor	Outer	1.792	–1.051
	Inner	1.364	–0.920
	Dome	1.605	–0.935
Inner Midplane		1.358	0.080

Information on electron temperature, electron density, heat load, and particle flux on divertor targets were provided by the EAST divertor Langmuir probe diagnostic system consisting of 89 groups of triple probes of which the poloidal layout is shown in Fig. 1.[11] The total distribution of radiated power in bulk plasma can be provided by four 16-channels AXUV (absolute extreme ultraviolet) detector arrays, in total 64 channels, installed in the horizontal port P, and one 24-channel AXUV array, installed in the upper-vertical port C.[12] Impurities, such as argon, deuterium, lithium, carbon, and tungsten, in the upper divertor region (only near inboard and outboard targets) can be observed by divertor tungsten spectroscopy with the range of 399–431 nm.[13] Moreover, these results are verified using the filterscope diagnostic system and a flat-field extreme ultraviolet (EUV) spectrometer with fast time resolution at the mid-plane.[14,15]

3. Results and discussions

As EAST upgraded its upper divertor into actively cooled W/Cu PFCs in 2014, the heating power simultaneously increased dramatically. Therefore, a considerably bigger heat load is supposed to be deposited on the divertor target. In this study, Ar seeding experiments were performed for controlling the heat flux onto the tungsten divertor target. In addition, the divertor radiation, asymmetry, and impurity transport are also investigated.

3.1. Heat load and radiation

The particle flux is related to ion saturation current density j_s, calculated by the equation

$$j_s = I_s/A_{pr}, \quad (1)$$

where I_s is the ion saturation current, acquired directly by Langmuir probes, and A_{pr} is the tip effective area (2.5 mm^2).

The heat flux to the target is also based on the measurement by the Langmuir probes. The parallel heat flux is given by

$$q_{\parallel} = \gamma_{sh} T_{et} k_B j_s / e, \tag{2}$$

where γ_{sh} is the total sheath heat transmission factor for deuterium plasma (~ 7, assuming $T_i = T_e$), T_{et} is the electron temperature at the divertor target, and k_B is the Boltzmann constant. Thus, the heat flux to the target is measured by

$$q_t = q_{\parallel} \sin \vartheta, \tag{3}$$

where ϑ is the grazing angle between the target and the incident magnetic field.[11,16]

Shot#57417 was an H-mode discharge with USN divertor configuration. The drift pointed toward the top divertor, and the divertor cry-pump was activated. In this shot, B_t was fixed at 2.3 T and I_p at 0.4 MA, and the heating power was fixed at approximately 4.3 MW with the ICRF of 1.5 MW and LHW of 2.8 MW. The upstream density (in separatrix), $n_{up,sep} = 1.0 \times 10^{19}$ m^{-3}, was measured by reflectometry. Ar impurity was seeded from the upper outboard target at the rate of 2.2–2.7 $\times 10^{20}$ e$^-$/s for 200 ms. After a delay time of 100 ms, the effect of Ar started at approximately 5.1 s. At the strike point, the ion saturation current j_s, measured by the divertor Langmuir probe, was decreased by 60%, and the electron temperature T_e decreased to less than 5 eV, because the ionization of the seeded neutral gas led to the increase of radiation to exhaust power in the divertor region.

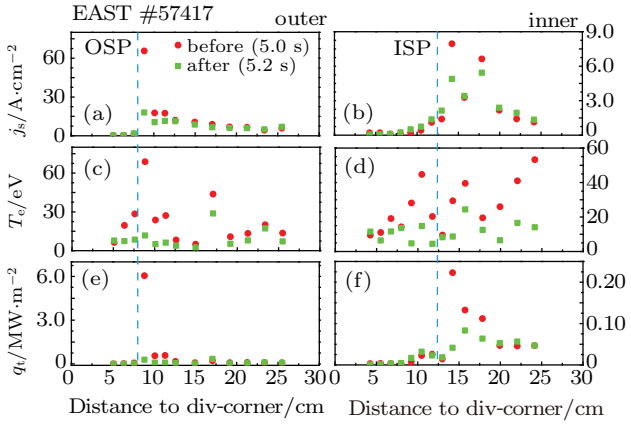


Fig. 2. (color online) Profiles of (a), (b) ion saturation current, j_s, (c), (d) electron temperature, T_e, and heat flux, q_t, on outer and inner divertor targets before (e), (f) and after Ar seeding. OSP: outer strike point; ISP: inner strike point. The clear error data are marked with circles.

More importantly, the heat flux, q_t, onto the outer divertor target plate, which once was more than 6 MW/m^2 with ELMy before Ar seeding, was clearly reduced to less than 0.5 MW/m^2. The plasma was completely detached (at and near the strike point) from the upper outboard target. During gas puffing, the increase of the radiated power measured using the AXUV was approximately 350 kW in total.

Figure 3 shows the profile of radiation obtained by the horizontal AXUV arrays. A burst of radiation in the upper and lower divertor regions led to the mitigation of ion and heat fluxes onto the divertor target. However, approximately 30% total radiation, ascribed to Ar impurity puffing, was distributed inside the core plasma region, which caused 5% loss of the entire plasma stored energy, and it rapidly returned to the initial state when the Ar puffing stopped. Nevertheless, for another discharge under similar plasma conditions (Shot #57423, Fig. 5) with the long pulse Ar seeding (1s), the results reveal a clear difference in the entire stored energy, which decreased by 32 kJ, $\sim$ 35%. Subsequently, an H- to L-mode transition was observed. The injection method is a key factor to the experimental results of the impurity seeding according to the experience of our device and other devices. For example, a single continuous long pulse Ar seeding, as shown in Shot #57423, easily causes Ar accumulation in the plasma core region, which is possibly of considerable risk to plasma confinement.

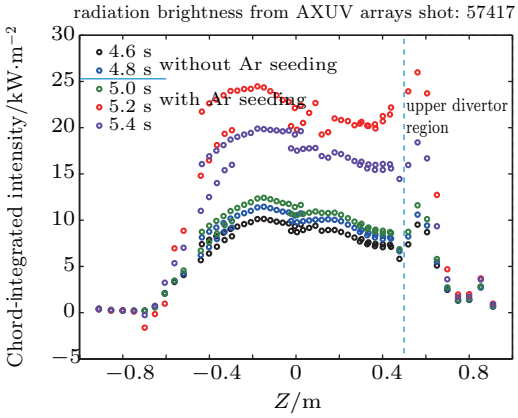


Fig. 3. (color online) Profile of radiation before and after Ar injection ($R = 1.85$ m).

3.2. Asymmetry

The divertor asymmetry for particle and heat fluxes depends on the divertor geometry and the magnetic equilibrium, as well as the plasma shape and parameters. There is a considerably strong in–out asymmetry with considerable difference for heat and particle fluxes between the inner and the outer targets in case of the present geometry in EAST. This asymmetry is clearly evident with the increase of plasma electron density, which is proved by the previous experimental results on the machine.[17]

Figure 4 shows the time evolution of plasma parameters for the preceding discharge #57417 using Ar seeding. The in–out asymmetry of ion saturation current and heat flux in the upper divertor region reduced significantly after Ar impurity seeding, which led to the detachment on the divertor target. The inner divertor first entered the detached state owing to less particle flow into the inner divertor region. Subsequently, the outer divertor followed the inner one to detachment.

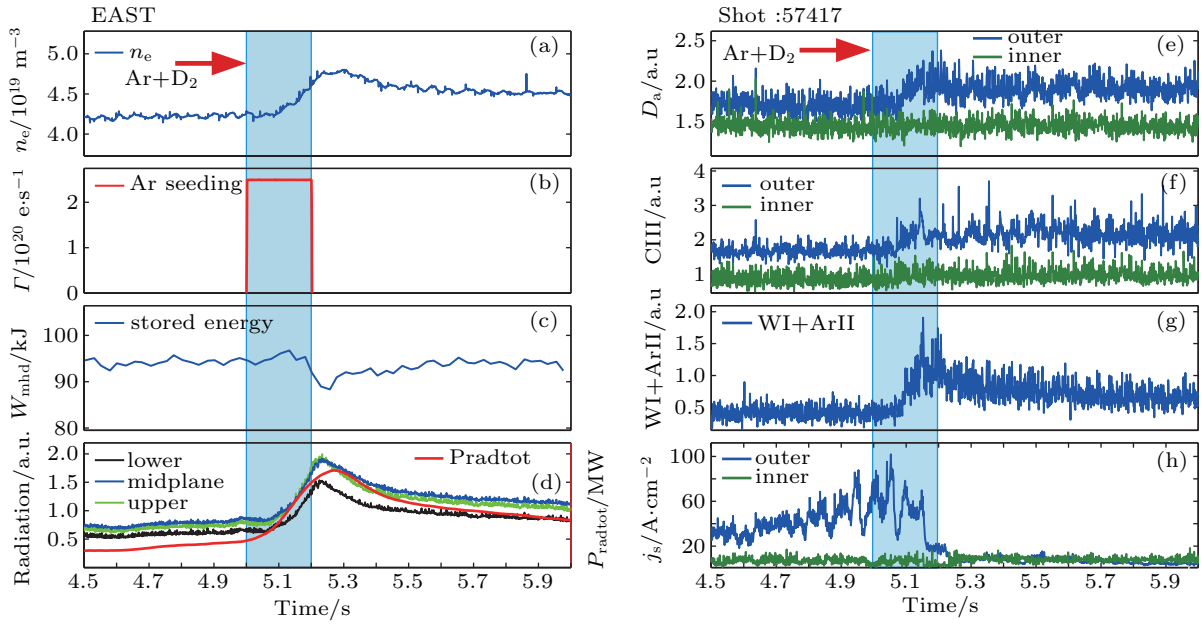


Fig. 4. (color online) Time traces of H-mode discharge with Ar seeding. The Ar mixture was seeded from the upper outer divertor target, and it started to function at 5.1 s owing to the delay of pipe length. (a) Plasma line-averaged density. (b) Ar/D_2 mixture seeding rate. (c) Stored energy of plasma. (d) Midplane, upper divertor, lower divertor region line integrated radiation, and total radiation power. (e), (f), (g) Emission intensities of impurity in the upper divertor region, measured using filterscope arrays. Note that the WI+ArII signal may contain two types of impurity: WI (400.87 nm) and ArII (401.38 nm), because the system cannot well distinguish these two spectral lines. (h) Ion saturation current in outer and inner divertor regions.

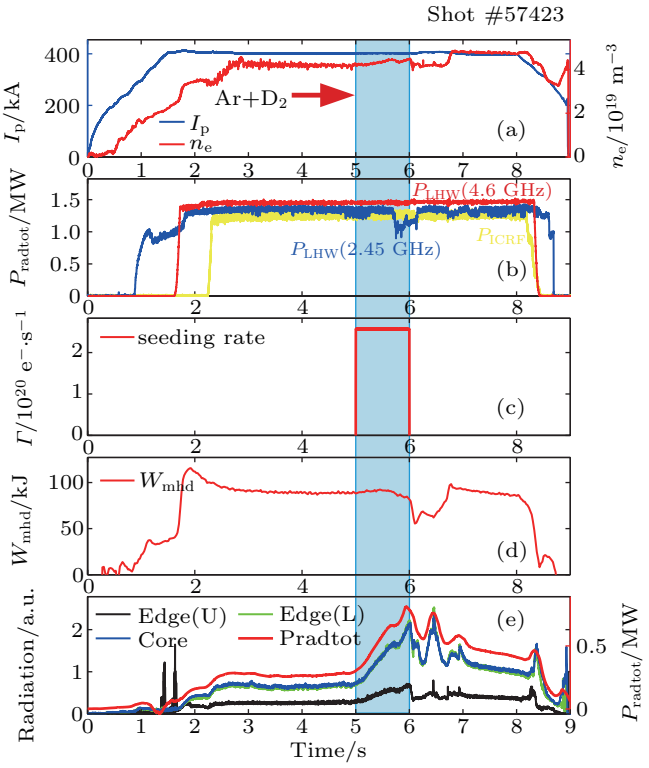


Fig. 5. (color online) Time evolution of Shot#57423. (a) Line integrated density (n_e) and plasma current (I_p). (b) Heating power: 2.45 GHz LHW, 4.6 GHz LHW and ICRF. (c) Impurity seeding rate. (d) Stored energy of plasma: W_{mhd}. (e) Core, upper divertor, lower divertor region line integrated radiation, and total radiation power.

Deuterium line emission is frequently used for evaluating the plasma characteristics such as the density, electron temperature, and the frequency of ELMs. As shown in Fig. 4, the D_α emission increases clearly in both inner and outer divertor regions after Ar injection, which is a sign of divertor detachment onset. The increase of D_α emission was attributed to the increased neutral fluxes. Generally, the D_α line emission exhibits higher photon efficiency in recombining plasmas at higher density and lower electron temperature.[17] These results were firstly found in the EAST ITER-like tungsten divertor to predict and validate the detachment process. To compare the differences between the lower carbon divertor and upper tungsten divertor, Ar impurity was seeded, respectively, from upper and lower divertor targets under similar plasma setting and heating conditions, corresponding to different divertor configurations: USN and LSN, respectively. Compared to the LSN configuration, the in–out asymmetry of the particle flux is smaller than the case under the USN condition. The primary reason is that the geometry shape is different for the upper divertor structure and lower divertor structure. Each of these two divertors exhibits different geometry shapes, which directly affects the divertor plasma parameters such as power flux, pumping efficiency, recycling coefficients, and neutral pressure.[18] From the above experiments, we observed that the distribution of plasma density in the two divertor regions is considerably different.[19] The results indicated that it is easier to achieve detachment on both inner and outer targets in the upper divertor than that in the lower divertor geometry.

3.3. Impurities

Impurities, such as Ar, C, Li, and W, may exist in the entire space of the vacuum chamber during EAST operations. In the divertor and SOL regions, it is beneficial for long pulse high performance discharges to bring in moderate impurity that plays an important role in power exhausting and acceler-

ating the plasma detachment process. Conversely, impurity in the core plasma region is harmful for the plasma confinement that may cause a considerable loss of stored energy, and then cause the plasma to go into the fluctuated state, even leading to bring disruption finally.

As Fig. 6 shows, the Ar concentration reached a considerably high level after the mixture was injected in the upper divertor region. Ar is a quite strong radiator when the electron temperature T_e is in the range of 10–40 eV. The electron temperature close to the targets is typically within this region. Therefore, the results reveal that the heat load and ion flux onto the divertor target decreased rapidly.

In Section 3.1, concentration of Ar ions in the core region that caused the increase of radiation therein was also confirmed by the EUV spectroscopy. The primary reason was attributed to the transport of the impurity ion along with $\nabla \boldsymbol{B}$ drift direction into the core region and the ionization there. The similar experiment conducted in DIII-D demonstrated that seeded Ar impurity accumulated in the core plasma with the $\boldsymbol{B} \times \nabla \boldsymbol{B}$-ion drift directed toward the X-point.[20–22]

As Ar gas was injected from the upper divertor target, there was a notable increase of C and Li signals accompanying the gradually increasing Ar impurity signal observed by the divertor impurity spectroscopy. After the peak signal of the Ar intensity was approximately 5.2 s, Li decreased gradually and C either decreased rapidly. This phenomenon was attributed to the increased Ar ions flux, which was accelerated to the target by the sheath potential and produced sputtering on plasma facing components, particularly on divertor targets under the strong Li coating conditioning. The decline of Li and C impurities was also ascribed to the decrease of Ar ions because the seeded Ar cooled the plasma in the divertor region, so that less Ar could be ionized. The similar results of CIII emission in the divertor region, which are measured using the filterscope system, confirmed the phenomenon as well.

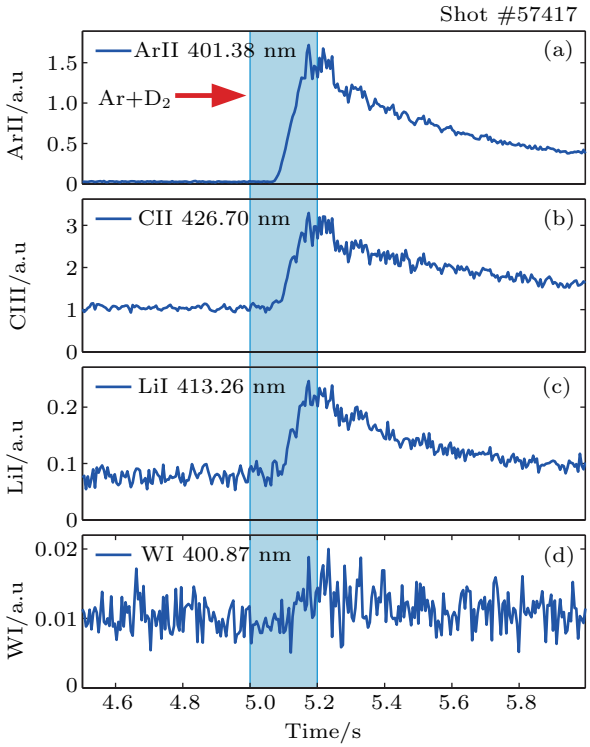


Fig. 6. (color online) Time trace of major types of impurity in upper divertor region: (a) Ar, (b) C, (c) Li, and (d) W, which were observed by divertor tungsten spectroscopy. There was no evident change of tungsten after Ar seeding in this shot.

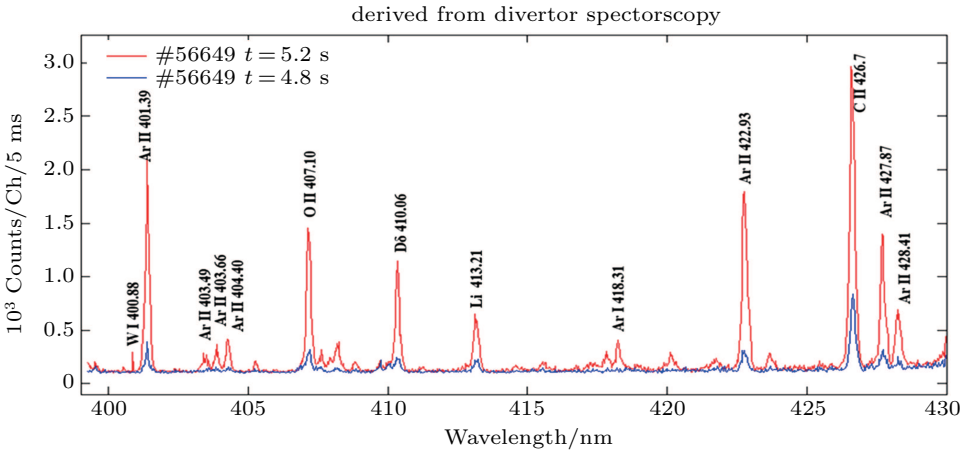


Fig. 7. (color online) Impurities in the upper divertor region observed by div-W spectroscopy without Ar seeding (4.8 s) and with Ar seeding (5.2 s). In this L-mode discharge, a small amount of tungsten sputtered from the divertor target, which causes a rapid increase of core radiation.

As is well known, EAST upgraded its upper divertor into actively cooled W/Cu PFCs in 2014, which consequently produced concern over how the W transport and concentration affect the plasma confinement. Typically, the tungsten sputtering was rarely observed by spectroscopy with strong Li-coating wall condition on the chamber surface. In the Shot#56649, an L-mode discharge with the LSN configuration, after Ar seeding, as shown in Fig. 7, the sputtered tungsten observed qualitatively by divertor tungsten spectroscopy, entered the core plasma and thus resulted in the degradation of plasma confinement owing to the burst of core radiation. Similar results for Ar seeding were discovered in ASDEX-Upgrade as well.[23,24]

As previously mentioned, it is deduced that the sputtering of tungsten is primarily ascribed to Ar impurity being ionized in the boundary plasma and accelerated to the target owing to sheath potential. However, the quantitative calibration of tungsten concentration is still in commissioning because the tungsten and argon signals exhibit an overlap in this wavelength range.

4. Summary

In this study, the radiative divertor behavior involving the heat flux, radiation, asymmetry, and impurities was investigated by using the Ar mixture as the radiator.

The asymmetry of the particle fluxes and heat loads between inner and outer divertor reduced significantly after Ar impurity injection. In addition, the respective Ar mixture gases were seeded, from the upper and lower (carbon) divertors under similar plasma setting and heating conditions. For the lower divertor, this asymmetry is smaller than that for the top one.

Moreover, impurities were investigated. It is proved that Ar is an efficient radiator. However, there will be the risk that Ar impurity contaminates core plasma and leads to a considerable decrease of plasma stored energy. The concentration of C and Li is associated closely with the Ar injection owing to the sputtering. Unlike the carbon divertor, Ar seeding produced tungsten sputtering on the surface of the PFCs, which was observed in the experiment, and exhibited a considerable influence on plasma confinement. These results will provide a reference for future investigation on ITER discharge in the scenario of radiative divertor experiments using tungsten plasma facing components.

References

[1] Reimold F, Wischmeier M, Bernert M, *et al*. 2015 *Nuclear Fusion* **55** 033004

[2] Kallenbach A, Bernert M, Beurskens M, *et al*. 2015 *Nuclear Fusion* **55** 053026

[3] Maddison G P, Giroud C, Alper B, *et al*. 2014 *Nuclear Fusion* **54**

[4] Nakano T and Team J T 2015 *Journal of Nuclear Materials* **463** 555

[5] Wan B. N, Li J G, Guo H Y, *et al*. 2015 *Nuclear Fusion* **55** 104015

[6] Yao D M, Luo G N, Zhou Z B, *et al*. 2016 *Physica Scripta* **2016** 014003

[7] Wang D S, Guo H Y, Shang Y Z, *et al*. 2013 *Plasma Science & Technology* **15** 614

[8] Guo H Y, Li J, Wan B N, *et al*. 2014 *Physics of Plasmas* **21** 056107

[9] Guo H Y, Li J, Gong X Z, *et al*. 2014 *Nuclear Fusion* **54** 013002

[10] Wang W 2015 *Upgrade of Gas Puffing System and Preliminary Results in EAST Radiative Divertor Experiment* (MS Dissertation) (Hefei: University of Chinese Academy of Sciences) (in Chinese)

[11] Xu J C, Wang L, Xu G S, *et al*. 2016 *Review of Scientific Instruments* **87** 083504

[12] Duan Y M, Hu L Q, Mao S T, *et al*. 2011 *Plasma Science & Technology* **13** 546

[13] Mao H, Ding F, Luo G N, *et al*. 2017 *Review of Scientific Instruments* **88** 043502

[14] Zhang L, Morita S, Xu Z, *et al*. 2015 *The Review of scientific instruments* **86** 123509

[15] Xu Z., Wu Z. W., Gao W., *et al*. 2016 *Review of Scientific Instruments* **87** 11D429

[16] Pitcher C S and Stangeby P C 1997 *Plasma Physics and Controlled Fusion* **39** 779

[17] Wang D, Guo H, Wang H, *et al*. 2011 *Physics of Plasmas* **18** 032505

[18] Loarte A 2001 *Plasma Physics & Controlled Fusion* **43** R183

[19] Liu S C, Guo H Y, Xu G S, *et al*. 2012 *Physics of Plasmas* **19** 042505

[20] Petrie T W, Brooks N H, Fenstermacher M E, *et al*. 2008 *Nuclear Fusion* **48** 045010

[21] Jackson G L, Murakami M, Staebler G M, *et al*. 1999 *Journal of Nuclear Materials* **266** 380

[22] Jackson G L, Murakami M, McKee G R, *et al*. 2002 *Nuclear Fusion* **42** 28

[23] Kallenbach A, Balden M, Dux R, *et al*. 2011 *Journal of Nuclear Materials* **415** S19

[24] Neu R, Kallenbach A, Sertoli M, *et al*. 2011 *Journal of Nuclear Materials* **415** S322